KeA1

CHINESE ROOTS
GLOBAL IMPACT

#### Contents lists available at ScienceDirect

#### Petroleum Science

journal homepage: www.keaipublishing.com/en/journals/petroleum-science



#### Original Paper

### Research on shell-side heat and mass transfer with multi-component in LNG spiral-wound heat exchanger under sloshing conditions



Xue-Ping Du <sup>a, b, \*</sup>, Guang-Lei Yu <sup>c</sup>, Ya-Cheng Xu <sup>a</sup>, Zhi-Jie Chen <sup>a</sup>, Nai-Liang Li <sup>a</sup>, Huan-Guang Wang <sup>a, \*\*</sup>

- <sup>a</sup> School of Low-carbon Energy and Power Engineering, China University of Mining and Technology, Xuzhou, 221116, Jiangsu, China
- <sup>b</sup> Key Laboratory of Thermo-Fluid Science and Engineering, MOE, Xi'an Jiaotong University, Xi'an, 710049, Shaanxi, China
- <sup>c</sup> Xi'an Aerospace Propulsion Test Technology Institute, Xi'an, 710100, Shaanxi, China

#### ARTICLE INFO

# Article history: Received 31 December 2022 Received in revised form 15 May 2023 Accepted 18 October 2023 Available online 19 October 2023

Edited by Jia-Jia Fei and Min Li

Keywords:
Spiral-wound heat exchanger
Sloshing conditions
Two-phase flow
Multi-component
Heat and mass transfer

#### ABSTRACT

The spiral-wound heat exchanger (SWHE) is the primary low-temperature heat exchanger for large-scale LNG plants due to its high-pressure resistance, compact structure, and high heat exchange efficiency. This paper studied the shell-side heat and mass transfer characteristics of vapor-liquid two-phase mixed refrigerants in an SWHE by combining a multi-component model in FLUENT software with a customized multicomponent mass transfer model. Besides, the mathematical model under the sloshing condition was obtained through mathematical derivation, and the corresponding UDF code was loaded into FLUENT as the momentum source term. The results under the sloshing conditions were compared with the relevant parameters under the steady-state condition. The shell-side heat and mass transfer characteristics of the SWHE were investigated by adjusting the component ratio and other working conditions. It was found that the sloshing conditions enhance the heat transfer performance and sometimes have insignificant effects. The sloshing condition is beneficial to reduce the flow resistance. The comprehensive performance of multi-component refrigerants has been improved and the improvement is more significant under sloshing conditions, considering both the heat transfer and pressure drop. These results will provide theoretical support for the research and design of multi-component heat and mass transfer enhancement of LNG SWHE under ocean sloshing conditions.

© 2023 The Authors. Publishing services by Elsevier B.V. on behalf of KeAi Communications Co. Ltd. This is an open access article under the CC BY-NC-ND license (http://creativecommons.org/licenses/by-nc-nd/4.0/).

#### 1. Introduction

The spiral-wound heat exchanger (SWHE) is widely used and is one of the key equipment in the process of natural gas extraction, liquefaction, and transportation. Because of its high-pressure resistance, compact structure and high heat exchange efficiency, the SWHE has become the preferred main low-temperature heat exchanger for large-scale LNG devices, which is widely used in petroleum, chemical, and other fields.

Regarding the influence of sloshing on the performance of SWHEs, Yu et al. (2019), Wu et al. (2019), Ren et al. (2018d) and Li et al. (2020) studied the influence of sloshing conditions on heat

*E-mail addresses:* xpdcumt@cumt.edu.cn (X.-P. Du), whg2013@cumt.edu.cn (H.-G. Wang).

transfer characteristics at different flow rates by experimental or numerical calculation methods, and compared with experimental and empirical formulas. The results showed that the sloshing condition deteriorates the heat transfer performance. Wang et al. (2016) proposed a mathematical model of an SWHE under sloshing conditions, and Yu et al. (2019) conducted experimental and numerical studies on heat transfer characteristics of two-phase flow with propane as a medium under sloshing conditions. The results showed that the sloshing also deteriorates the performance. The research results of Ren et al. (2018b) showed that the increase in the sloshing frequency and amplitude would worsen the heat transfer, and the influence of sloshing frequency and amplitude on heat transfer performance was more obvious than that of other parameters, such as flow rate and pressure, among which the amplitude had the greatest influence. Ren et al. (2018a, 2022) also added the sloshing parameter as a momentum source term to the control equation to study the shell-side heat transfer and pressure

<sup>\*</sup> Corresponding author.

<sup>\*\*</sup> Corresponding author.

drop characteristics of superheated steam in the SWHE. The results indicate that the periodic sloshing has a significant impact on pressure drop and heat transfer performance, and the amplitude of oscillation has a greater impact on heat transfer performance than the influence of the period. Most sloshing conditions can improve the heat transfer performance (Ren et al., 2018a, 2022), which is contrary to the results of other researchers (Ren et al., 2018c).

The results of Yan et al. (2019) indicate that sloshing causes temperature increases and pressure fluctuations in SWHEs. Duan et al. (2016) proposed a dynamic model of multiphase flow SWHE under sloshing based on the moving boundary method and believed that the overall performance degradation of the SWHE due to sloshing was within 5% in most cases. Sun et al. (2021) believed that sloshing would periodically affect pressure drop and heat transfer coefficient, and the higher the sloshing frequency, the more significant the influence would be (Sun et al., 2019d). Pitching motion has a greater influence on the shell-side pressure fluctuation than other sloshing conditions. The increase of the pitching period and angle will increase the pressure fluctuation (Sun et al., 2019c). Under the sloshing condition, the pressure drop characteristics of vapor-phase mixed refrigerant are more affected (Sun et al., 2017), and the influence of fluctuation and pitch motion on the pipe-side pressure drop characteristics is greater than that of fluctuation and yaw (Ding et al., 2017a).

Han et al. (2017) studied the influence of the sloshing conditions on liquid film thickness through numerical calculation, and the results showed that sloshing conditions would worsen the uniformity of liquid film and make it unstable, thus weakening the heat transfer performance (Han et al., 2019). Duan et al. (2017) proposed a model to predict the thermal characteristics of SWHEs based on liquid migration, which can well simulate the thermal performance of SWHEs under sloshing conditions. The deviation between the calculation and experiment is within 4.5% during the sloshing amplitude of  $0-9^\circ$  and the period of 6-15 s.

On the whole, the experimental results show that the temperature will rise and the heat transfer performance will decrease under the condition of sloshing, while the numerical results show that the sloshing sometimes will strengthen the heat transfer performance while sometimes deteriorating it. Focusing on the multi-component heat and mass transfer laws, this paper will study the influence of the sloshing condition on the multi-component heat and mass transfer performance and resistance characteristics by comparing it with the static conditions. The research contents and technical route of this paper are shown in Fig. 1. The research results will provide theoretical support for the enhancement and design application of multi-component heat and mass transfer in

liquefied natural gas spiral-wound heat exchangers (LNG SWHEs) under ocean sloshing conditions.

#### 2. Model

#### 2.1. Sloshing model

#### 2.1.1. Sloshing instructions

The sloshing of the SWHE on the ships at sea is very complicated due to the SWHE is cylindrical. For a certain section, it can be divided into the cyclical movement of the water surface up and down and the sloshing caused by sloshing along the sides of the longitudinal axis of the ship, as shown in Figs. 2 and 3. Both motions show sinusoidal motion with the sea. Assume that the amplitude of the up-and-down undulation motion is  $A_Z$  and the period is  $T_Z$ ; the swing motion has a swing angle of  $\alpha$ , a swing arm of l and a period of  $T_X$ .

The actual motion of the SWHE at sea is a complex coupled motion composed of two motions. Two different motion periods lead to a complex trajectory of the composite motion, and there is also an initial phase angle  $\varphi$  in the cycle of the two motions. Figs. 4–7 are schematic diagrams of the composite motion trajectory of two different cycles and phase angle  $\varphi$  motion.

From the figure, it can be seen that the reciprocal route can just coincide when the phase angle  $\varphi$  of the two motions is 1/4 of the minimum common period of the two motions. The larger the minimum common period of the two motions, the more complicated the trajectory of the motion. When the actual hull moves with the wave, the hull is not perpendicular to the water surface, there is a lag time, and this time is the phase angle of two kinds of motion. This time is the phase angle of the two motions. The period of the

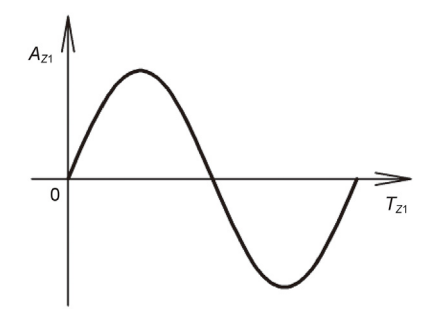


Fig. 2. Up and down motion.

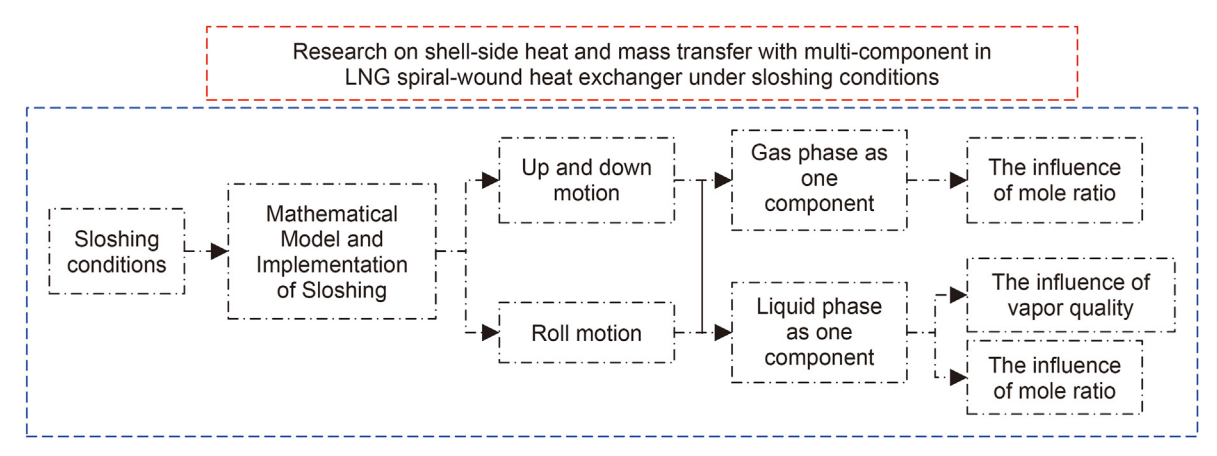


Fig. 1. Research content and technical route of this paper.

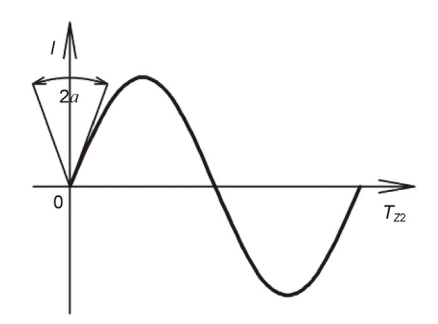
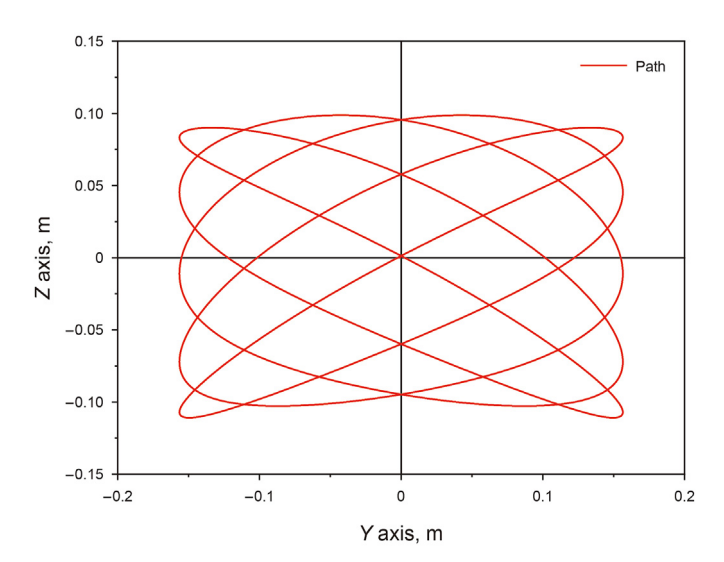
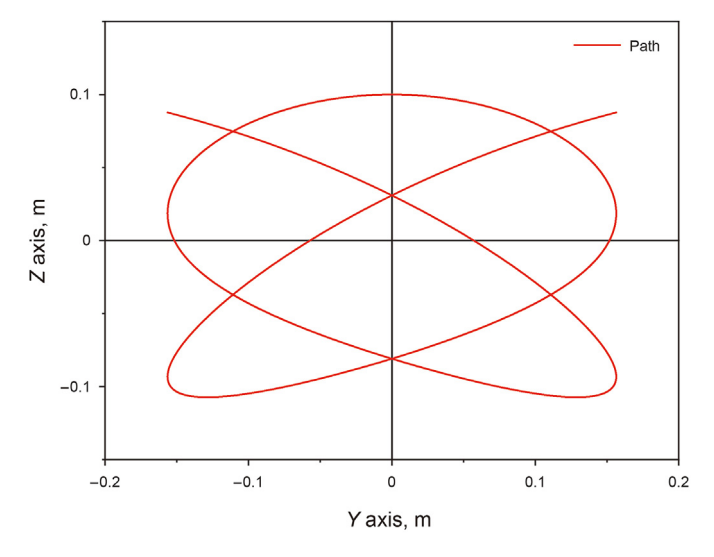


Fig. 3. Roll motion.



**Fig. 4.** Path with  $T_{Z1}=5$  s,  $T_{Z2}=4$  s,  $\varphi=0$ .



**Fig. 5.** Path with  $T_{Z1} = 5$  s,  $T_{Z2} = 4$  s,  $\varphi = \pi/2$ .

hull rocking is not synchronized with the wave period, which causes the period of the two motions to be out of synchronization.

#### 2.1.2. Mathematical models

Suppose the direction of travel of the boat is *X* direction and the

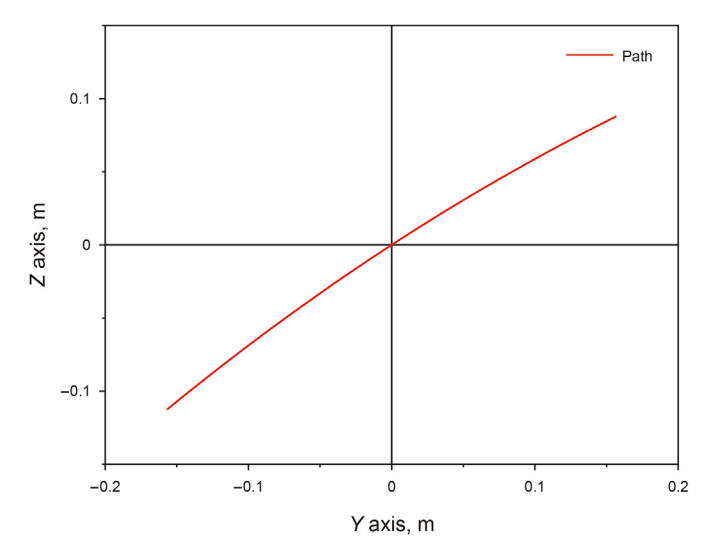


**Fig. 6.** Path with  $T_{Z1} = 5$  s,  $T_{Z2} = 5$  s,  $\varphi = 0$ .

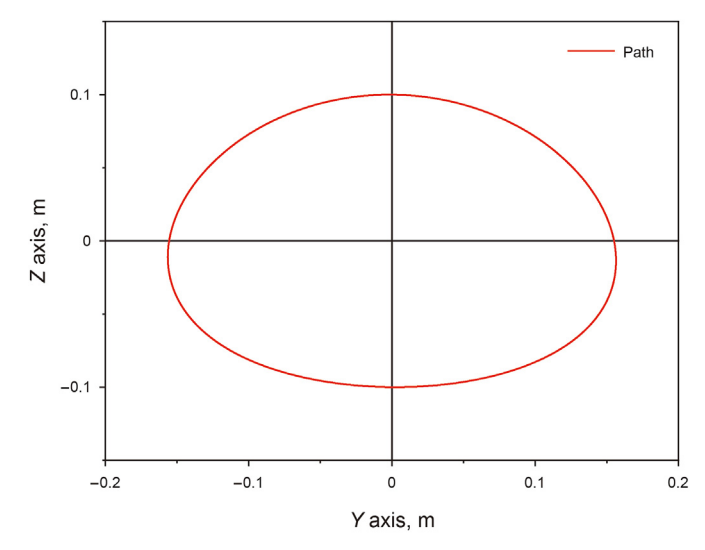


**Fig. 7.** Path with  $T_{Z1} = 5$  s,  $T_{Z2} = 5$  s,  $\varphi = \pi/2$ .

direction perpendicular to the horizontal plane is *Z* direction, as shown in Fig. 8. Then the mathematical model of wakes can be derived in the standard Cartesian coordinate system.

Firstly, the up and down undulating motion is decomposed, and the boat motion is always on the *Z*-axis during the undulating motion, and the displacement of the boat on the *Z*-axis as a function of time is:

$$L_{Z1} = A_Z \sin\left(\frac{2\pi}{T_Z}t\right) \tag{1}$$

Then, when moving up and down, the velocity of the boat on the *Z* axis over time is the function of:

$$v_{Z1} = A_Z \frac{2\pi}{T_Z} \cos\left(\frac{2\pi}{T_Z}t\right) \tag{2}$$

The acceleration of the boat on the *Z*-axis as a function of time during the up-and-down undulating motion is:

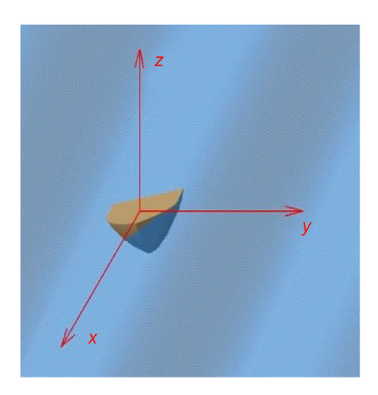


Fig. 8. Coordinate system.

$$a_{Z1} = A_Z \left(\frac{2\pi}{T_Z}\right)^2 \sin\left(\frac{2\pi}{T_Z}t + \pi\right) \tag{3}$$

Secondly, the swinging motion of the boat can also be decomposed, assuming that the swinging motion is in the plane perpendicular to the *X*-axis, i.e., the *YZ*-plane, the length of the swing arm is l, the swing angle is  $\pm \alpha$ , and the period is  $T_X$ . The displacement of the boat in the *Y*-axis as a function of time during the swinging motion is:

$$L_{Y2} = l \sin\left(\alpha \sin\left(\frac{2\pi}{T_X}\right)t\right) \tag{4}$$

The displacement component of the swing motion in the *Z*-axis as a function of time is:

$$L_{Z2} = l \left( 1 - \cos \left( \alpha \sin \left( \frac{2\pi}{T_X} t \right) \right) \right)$$
 (5)

The velocity component of the oscillating motion in the *Y*-axis as a function of time is:

$$L_{Z1} = A_Z \sin\left(\frac{2\pi}{T_Z}t\right) \tag{6}$$

The velocity component of the oscillating motion in the *Z*-axis as a function of time is:

$$v_{Z2} = \alpha l \frac{2\pi}{T_X} \cos\left(\frac{2\pi}{T_X}t\right) \sin\left(\alpha \sin\left(\frac{2\pi}{T_X}t\right)\right)$$
 (7)

The acceleration component of the oscillation motion in the *Y*-axis as a function of time is:

$$a_{Y2} = -\alpha l \frac{2\pi^2}{T_X} \sin\left(\frac{2\pi}{T_X}t\right) \cos\left(\alpha \sin\left(\frac{2\pi}{T_X}t\right)\right) - \alpha^2 l \left(\frac{2\pi}{T_X}\right)^2 \cos^2\left(\frac{2\pi}{T_X}t\right) \sin\left(\alpha \sin\left(\frac{2\pi}{T_X}t\right)\right)$$
(8)

The acceleration component of the oscillation motion in the *Z*-axis as a function of time is:

$$a_{Z2} = -\alpha l \frac{2\pi^2}{T_X} \sin\left(\frac{2\pi}{T_X}t\right) \sin\left(\alpha \sin\left(\frac{2\pi}{T_X}t\right)\right) + \alpha^2 l \left(\frac{2\pi}{T_X}t\right)^2 \cos^2\left(\frac{2\pi}{T_X}t\right) \cos\left(\alpha \sin\left(\frac{2\pi}{T_X}t\right)\right)$$
(9)

Finally, the gravitational acceleration of the boat as it swings is decomposed, and the gravitational acceleration as a function of time on the *Y*-axis is:

$$a_{Y3} = -g \sin\left(\alpha \sin\left(\frac{2\pi}{T_X}t\right)\right) \tag{10}$$

The gravitational acceleration in the *Z*-axis as a function of time is:

$$a_{Z3} = -g \sin\left(\alpha \cos\left(\frac{2\pi}{T_X}t\right)\right) \tag{11}$$

The acceleration generated during sloshing will be loaded in the equation with the source term when solving the momentum equation. Thus, the source term of momentum in the *Y* direction is the product of the sum of the acceleration components of up and down undulating motion, swaying motion and gravity with sloshing in the *Y* direction and the density, i.e:

Source<sub>Y</sub> = 
$$\rho(a_{Y1} + a_{Y2} + a_{Y3})$$
 (12)

Bringing Eqs. (8) and (10) into the above equation gives the momentum source term of the *Y*-axis as:

Source<sub>Y</sub> = 
$$\rho \left( 0 - \alpha l \left( \frac{2\pi}{T_X} \right)^2 \sin \left( \frac{2\pi}{T_X} t \right) \cos \left( \alpha \sin \left( \frac{2\pi}{T_X} t \right) \right) + a_{Y3} \right)$$
  
 $- \alpha^2 l \left( \frac{2\pi}{T_X} \right)^2 \cos^2 \left( \frac{2\pi}{T_X} t \right) \sin \left( \alpha \sin \left( \frac{2\pi}{T_X} t \right) \right)$   
 $- g \sin \left( \frac{2\pi}{T_X} t \right)$ 
(13)

Similarly, the momentum source term in the Z-direction is also the product of the acceleration of each motion in the Z-axis and the density, and the momentum source term in the Z-axis can be obtained by substituting Eqs. (3), (9) and (11):

Source<sub>Y</sub> = 
$$\rho(a_{Z1} + a_{Z2} + a_{Z3})$$
 (14)

Source<sub>Z</sub> = 
$$\rho \left( A_Z \left( \frac{2\pi}{T_Z} \right)^2 \sin \left( \frac{2\pi}{T_X} t + \pi \right) - \alpha l \frac{2\pi^2}{T_X} \sin \left( \frac{2\pi}{T_X} t \right) \sin \left( \alpha \sin \left( \frac{2\pi}{T_X} t \right) \right) - g \sin \left( \alpha \cos \left( \frac{2\pi}{T_X} t \right) \right) \right)$$
 (15)

#### 2.1.3. Computational model

The sloshing parameters obtained from the above solution are used as momentum source terms, and the sloshing conditions can be realized by loading them into the momentum equations of the FLUENT computational domain using the UDF code. The sloshing parameters in the laboratory are usually constrained (Sun et al., 2017, 2019a, 2019b; Yan et al., 2019; Yu et al., 2019) because of the test rig and other reasons, and their parameter ranges are shown in Table 1. In this paper, to study the influence of the sloshing parameters, the parameters selected concerning the study of Ren et al. (2018a) are shown in Table 2.

#### 2.2. Mass transfer model

#### 2.2.1. Governing equations in the shell-side of the SWHE

The shell-side heat transfer of the SWHE contains both sensible and latent heat (evaporation and boiling). The numerical calculation process includes the solution of the flow field and temperature

field, and the flow field includes the multiphase flow model and Reynolds time-averaged turbulence model. One of the multiphase flow models uses the VOF model to trace the vapor-liquid intersection. For incompressible flows, the VOF model is mainly used to calculate the continuity equation for the gas-liquid phase, and the calculations also include the CSF model (Brackbill et al., 1992) for dealing with the tension and contact angle at the gas-liquid interface. The results obtained from the CSF calculations will be loaded into the N–S equation as the source term of the momentum equation.

The governing equations on the shell side of the SWHE mainly include the continuity equation, momentum equation, and energy equation. Due to the VOF multiphase flow model, the model assumes that the total volume of the liquid zone and the vapor zone are constant and satisfy the continuity equation. Since the mass transfer model involves mass transfer and heat transfer, the decomposition corresponds to the source terms in the three equations. About the CSF model, the content can be referred to as the reference (Brackbill et al., 1992).

The governing equations are below, firstly, the continuity equation.

$$\nabla \cdot \boldsymbol{u} = 0 \tag{16}$$

The volume fraction equation is below.

$$\frac{1}{\rho_{\text{vap}}} \left[ \frac{\partial}{\partial t} (\alpha_{\text{vap}} \rho_{\text{vap}}) + \nabla \left( \alpha_{\text{vap}} \rho_{\text{vap}} \overrightarrow{\nu}_{\text{vap}} \right) = S_{\alpha_{\text{vap}}} + \sum_{\text{liq}=1}^{n} (\dot{m}_{\text{lv}} - \dot{m}_{\text{vl}}) \right]$$
(17)

The properties appearing in the transport equations are determined by the presence of the component phase in each control volume. In this paper, VOF model is used, and the density in each cell is given by

$$\rho = \alpha_{\text{liq}} \, \rho_{\text{liq}} + \left(1 - \alpha_{\text{liq}}\right) \rho_{\text{vap}} \tag{18}$$

A single momentum equation is solved throughout the domain, and the resulting velocity field is shared among the phases. The momentum equation, shown in Eq. (19), is dependent on the volume fraction of all phases through the properties  $\rho$  and  $\mu$ .

$$\frac{\partial}{\partial t}(\rho \mathbf{v}) + \nabla \cdot (\rho \mathbf{v} \mathbf{v}) = -\nabla p + \nabla \cdot \left[ \mu \left( \nabla \mathbf{v} + \nabla \mathbf{v}^T \right) \right] + \rho \mathbf{g} + \mathbf{F}$$
 (19)

The energy equation is below.

$$\rho \frac{D}{Dt} \left( \boldsymbol{e} + \frac{1}{2} \boldsymbol{u} \cdot \boldsymbol{u} \right) = \nabla \cdot (\boldsymbol{\Sigma} \cdot \boldsymbol{u}) + \rho \boldsymbol{u} \cdot \boldsymbol{f} - \nabla \cdot \boldsymbol{q}$$
 (20)

In the Lee model (Lee, 1979), the liquid-vapor mass transfer (evaporation and condensation) is governed by the vapor transport equation.

$$\frac{\partial}{\partial t} (\alpha_{\text{vap}} \rho_{\text{vap}}) + \nabla \cdot \left( \alpha_{\text{vap}} \rho_{\text{vap}} \overrightarrow{V}_{\text{vap}} \right) = \dot{m}_{\text{lv}} - \dot{m}_{\text{vl}}$$
 (21)

The energy equation mainly solves for the temperature field, and the heat transfer in the SWHE contains two main dimensions, diffusion, and convection. The mass transfer process not only has an

**Table 1** Parameter range of sloshing.

<i>A</i> <sub>Z1</sub> , mm	<i>T</i> <sub>Z1</sub> , s	L, mm	α, °	<i>T</i> <sub>Z2</sub> , s
80-250	3-30	800-1500	9	5-20

**Table 2** Actual parameter of sloshing.

$A_{Z1}$ , mm	<i>T</i> <sub>Z1</sub> , s	L, mm	α, °	<i>T</i> <sub>Z2</sub> , s
100	5	1000	9	5

effect on the continuity equation, but also the standard state enthalpy set by the material properties in the mass transfer process contains the latent heat from the phase change process, so the mass transfer process also contains the heat transfer process, and it will still return to the energy equation with the enthalpy difference of the work material.

As shown in Fig. 9, the usual control body discrete cell grid contains three states: liquid phase, gas phase, and mixed-phase, as shown in the example of sheet flow. Therefore, the volume fraction  $\alpha$  of the liquid phase in the grid corresponds to 0, 1, and  $0 < \alpha < 1$ . The volume fraction of the control body discrete cell grid is multiplied by the volume to obtain the effective liquid phase refrigerant volume in the superheated state. Finally, the volume of the liquid-phase refrigerant in all superheated states in the computational domain is obtained by summing up all the discrete cell grids of the control body.

The flow and temperature fields are first calculated by initialization, and then the temperature-weighted liquid-phase refrigerant volume *vol* in the superheated state, and the outlet liquid-phase and vapor-phase temperatures are calculated.

#### 2.2.2. Model implementation

To make the improved mass transfer model operational, a UDF function is used in the FLUENT software. The processes and judgments are calculated by calling the function macro DEFINE\_ADJUST (name, domain) from the FLUENT function library. Then by calling the non-linear mass transfer macro DEFINE\_MASS\_TRANSFER updates the source terms of the mass transfer to the N—S equation and the energy equation.

Computationally heavy tasks are assigned to the computational nodes through a parallelization process, then passed to HOST nodes and summarized through a transfer function, and finally passed to the CORTEX. In this way, the computing tasks of each node are even and the computing efficiency is improved. In addition, the overall computation speed can also be improved by controlling a certain time step to update the iterative computation relaxation factor. After the relaxation time is obtained for a single calculation within

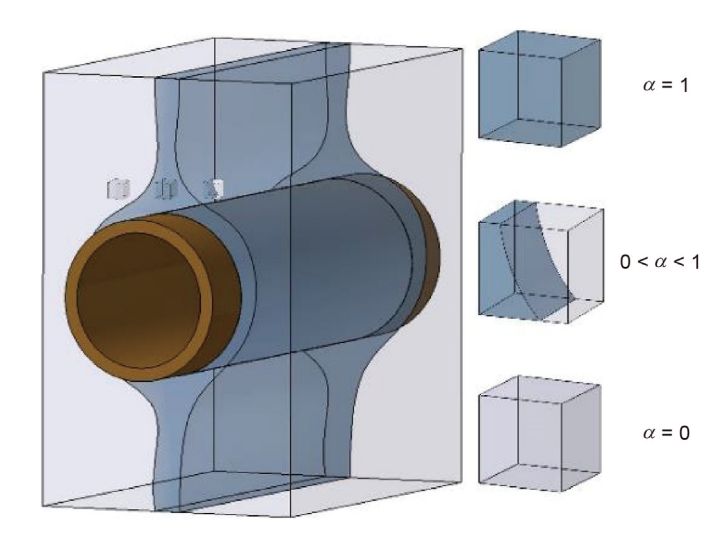


Fig. 9. Sketch of sheet flow pattern.

a time step, the minimum computation amount can be achieved by using a static storage call and other functions when traversing other grids, which can also improve the overall computation speed.

#### 2.3. Model validation

#### 2.3.1. Computational models and methods

The multi-component model in the present paper is validated by the experimental data from Hu et al. (2019). In the experiment, the shell-side heat and mass transfer of a two-phase hydrocarbon refrigerant mixture under a boiling flow of the SWHE were studied. The experimental data from the literature were simulated and validated with the model parameters shown in Table 3.

In order to simplify the calculation, periodic units were extracted from the experimental model (shown in Fig. 10) for calculation, and the extracted model is shown in Fig. 11. The spiral tubes of the SWHE are staggered with left-handed and right-handed in each layer. The model was optimized to improve the calculation accuracy, reduce the amount of calculation, and simulate the actual import and export boundary conditions as much as possible. Firstly, the whole control body is divided into a left-handed discrete domain and a right-handed discrete domain and the structured mesh is divided separately, which can greatly improve the mesh quality and increase the calculation accuracy, and the computational amount of structured mesh is relatively low under the same number of grids. Secondly, two separate discrete domain coupling parts use the INTERFACE boundary for data transmission to realize the grid partition of the whole control body.

The computational boundary is shown in Fig. 11. The computational domains on both sides are completely rotationally symmetric. The vapor and liquid enter from the inlet, the vapor refrigerant enters from the middle of the winding tube, and the liquid refrigerant enters from the upper part of the winding tube. The first winding tube at the bottom serves as a diversion tube, which is the transition tube guiding the uniform distribution of refrigerant and the boundary of the adiabatic wall. The four winding tubes under the right guide tube are wall boundaries with constant heat flow density, and according to the experimental model, only half of the winding tubes with constant heat flow density in the discrete domain and the remaining half are insulation boundaries. The front and back of the control body are symmetric boundaries, while the left and right are periodic boundaries. The liquid can circulate across the winding tubes. The outlet is the pressure outlet boundary.

The k- $\omega$  turbulence model with a low Reynolds number is used for calculation. The VOF multiphase flow model, species transport model, and the improved UDF mass transfer model are used in the mass transfer term and the mass transfer components. The second-order upwind discrete precision and coupled algorithm are used to solve the problem.

#### 2.3.2. Grid independence verification

In order to verify the grid independence of the calculation results, a random working condition is selected from the

**Table 3** Parameter of the model.

Parameter	Value	Unit
Angle of inclination	4	۰
Radial spacing	14	mm
Axial spacing	16	mm
The outer diameter of the tube	12	mm
The inside diameter of the tube	6	mm
Length of tube	160	mm

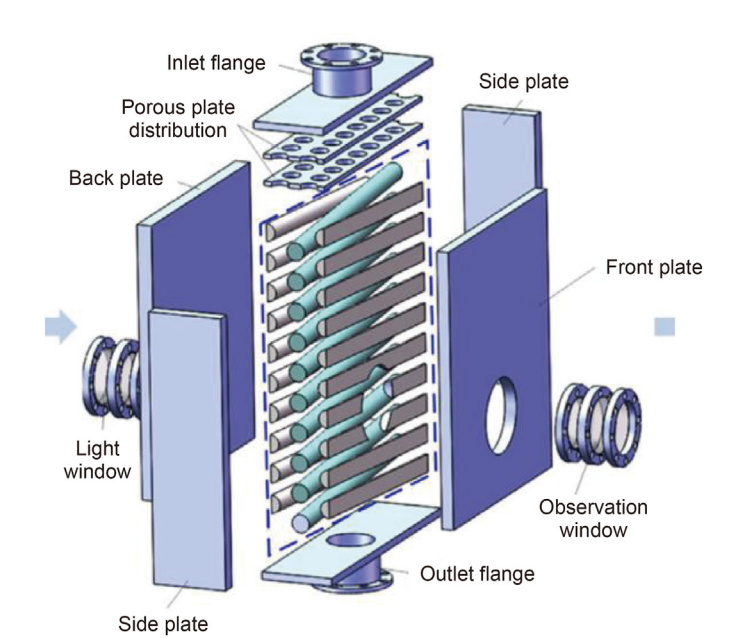


Fig. 10. Experiment model (Hu et al., 2019).

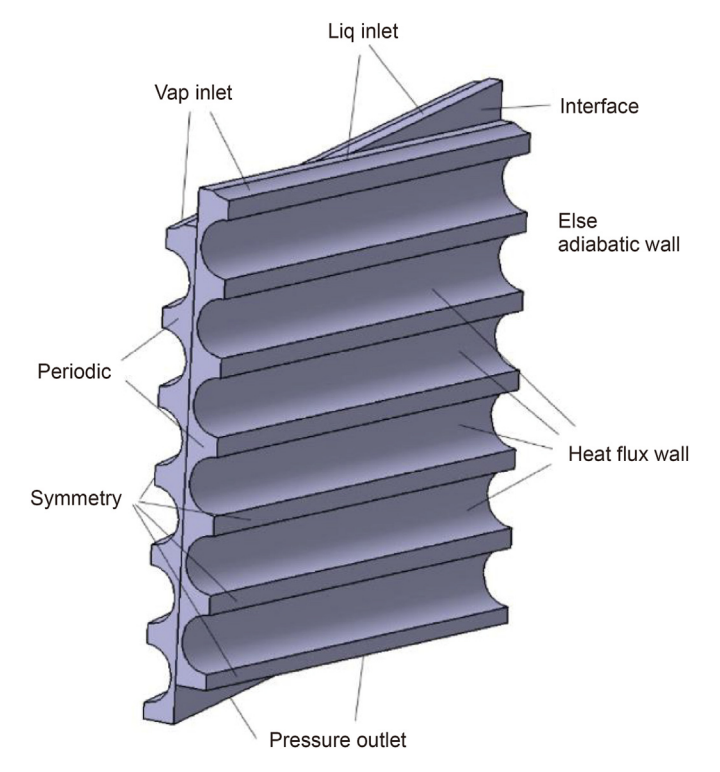


Fig. 11. The model and boundary.

experimental conditions (Hu et al., 2019) for verification. ICEM is used to divide the model into a hexahedral structured mesh. By encrypting the winding tube wall and the core area, five different mesh models are obtained. The relationship between the wall temperature and the heat transfer coefficient with the number of grids is obtained through calculation, respectively, as shown in Figs. 12 and 13.

#### 2.3.3. Model validation

In order to validate the reliability of the multi-component mass

transfer model, the experimental data and simulation of Hu et al. (2019) are compared and validated. Twenty-four different operating conditions are selected for calculation, as shown in Fig. 14. The maximum positive deviation from the experimental results is +13.5%, and the maximum negative deviation is -9.5%. The accuracy range of the fitting formula of Ding et al. (2018, 2017b) is  $-30\% \sim +50\%$ . Hu et al. (2019) improve the fitting accuracy based on Ding et al. (2018, 2017b), and its accuracy range is  $\pm25\%$ . The use of the improved multi-component mass transfer model proposed in this paper significantly improves the computational accuracy.

#### 3. Results and discussion

In order to study the influence of sloshing conditions on the shell-side multi-component heat and mass transfer performance of the SWHE. Firstly, the influences of various components on the heat transfer coefficient, relaxation time, and pressure drop of the SWHE are studied. Secondly, the sloshing condition is mathematically derived to obtain the sloshing model of the simulated seawater sloshing condition. Finally, the model is loaded into FLUENT software through the UDF interface and used as the source term of the momentum equation. The comparison between the sloshing condition and the static condition is added to study the influence of component proportion on the heat transfer performance in the two different states of wobble and static. The second component was divided into the influence of component proportion in the vapor phase on the heat transfer performance, the influence of vapor quality in the liquid phase on the heat transfer performance, and the influence of component proportion in the liquid phase on the heat transfer performance.

## 3.1. Influence of component proportion on heat transfer performance when the second component is a gas phase

When the first component of the gas-liquid mixed refrigerant is propane and the second component of the ethane is always in the gas phase. In order to study the influence of the proportion of the second component on the heat transfer performance, a multicomponent mass transfer model is used to study the shell-side heat and mass transfer of the multi-component gas-liquid mixed refrigerant on the SWHE.

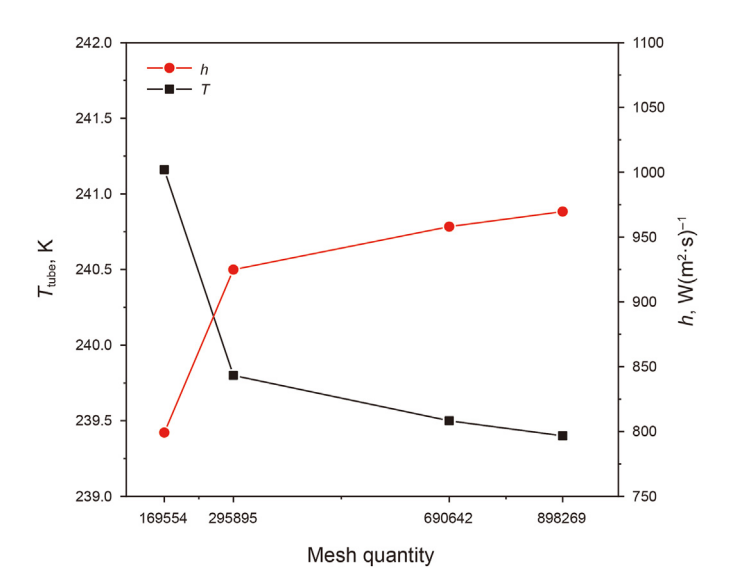


Fig. 12. h with different grid quantity.



Fig. 13. Grid.

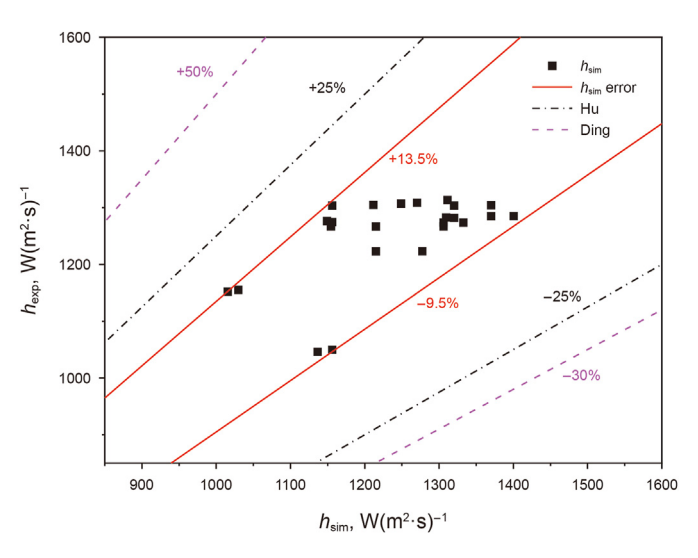


Fig. 14. Deviations between simulation and experiment.

Firstly, the mole fraction of the second component of ethane is adjusted to the range from 0% to 45% by controlling the flow rate of the liquid refrigerant unchanged. At this time, ethane accounts for the mass fraction of the corresponding gas phase refrigerant in the range of 0%–92%. Secondly, the influence of adding sloshing conditions on the shell-side heat and mass transfer and pressure drop performances of the SWHE are studied.

The calculated results are shown in Figs. 15—17. With the increase of the second component of the ethane, the heat transfer

coefficient increases gradually from 1155.2 to 1369.1  $W(m^2 \cdot K)^{-1}$ , nearly linear increase.

The higher the proportion of ethane in the gas phase, the higher the heat transfer efficiency, which is caused by the physical parameters of ethane. Compared with propane, ethane vapor has a lower density and higher viscosity. Therefore, as the proportion of ethane increases, the flow rate of vapor gradually increases, which can accelerate the flow of liquid refrigerant. Fig. 18 shows the gasliquid interface-free surface where the liquid refrigerant uniformly covers the heat transfer tube. It can be seen from the figure that as the refrigerant flows down the winding tubes, a uniform liquid film is formed on the tube wall and the liquid film gradually breaks with the flow. This is because as the refrigerant flows, phase change mass transfer causes the downward flow of the refrigerant to gradually decrease. Moreover, it can be seen from the figure that the manifold tends to transition from a sheet flow at the top to a cylindrical flow near the outlet.

The heat transfer performance is slightly improved and the pressure drop is reduced by increasing the sloshing conditions. With the increase of the sloshing condition, the heat transfer coefficient and relaxation time both increase to some extent with the increase of the ethane mole fraction, and the increase ratio ranges from 3.6% to 4.6%. This result is the same as the conclusion of Ren et al. (2018c). This is because under such working conditions, sloshing can make liquid film coverage more uniform and improve the uniformity of liquid film coverage. Wang et al. (2016) also put forward a similar view for this conclusion. After increasing the sloshing condition, the pressure drop is slightly reduced, and with the increase of the mole fraction of ethane, the pressure drop decreases by about -4.3% to -3.1%. This may be due to the presence of a laterally acting momentum consistent with the direction of the winding tube under the sloshing condition, which increase the lateral flow of the liquid refrigerant along the wall of the winding tubes. The staggered arrangement between the winding tube layers makes the flow area at any transverse section of the control body not the same, but presents periodic changes. Therefore, the momentum along the winding tubes increased by sloshing helps to increase the lateral migration of the liquid refrigerant and slightly reduce the pressure drop.

Increasing the mole fraction of ethane can improve the heat transfer coefficient, but also increase the pressure drop. Therefore, the comprehensive performance evaluation of the heat transfer

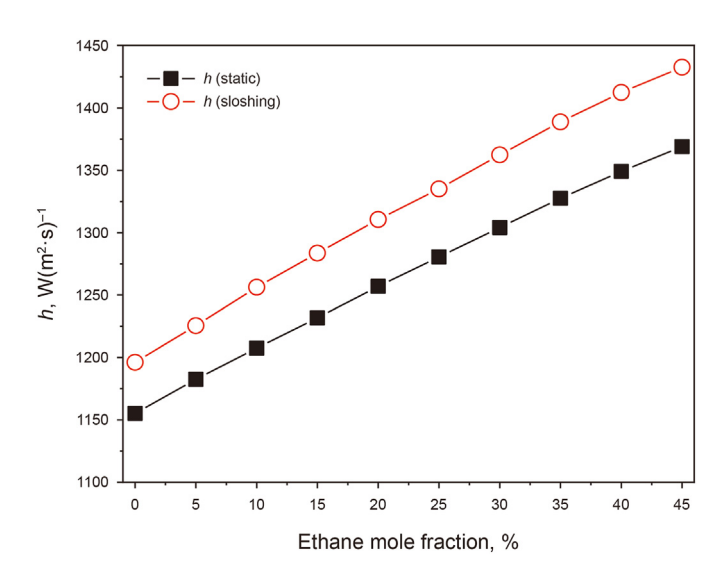


**Fig. 15.** *h* with ethane mole fraction.

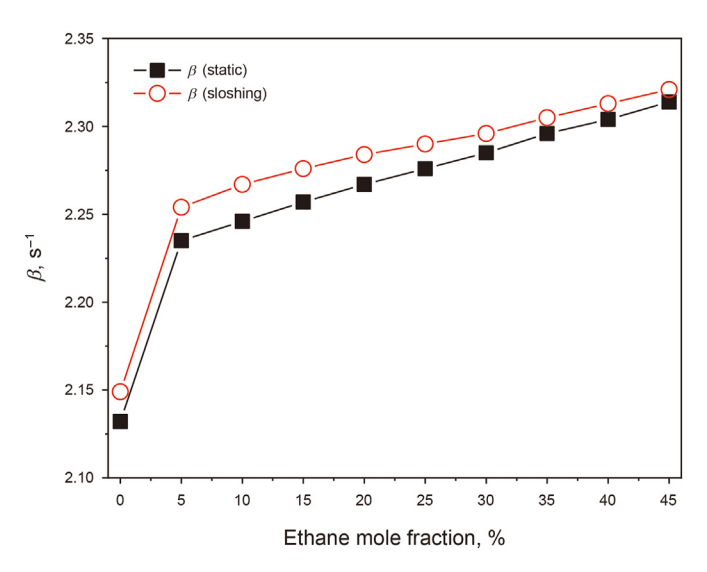


**Fig. 16.**  $\beta$  with ethane mole fraction.

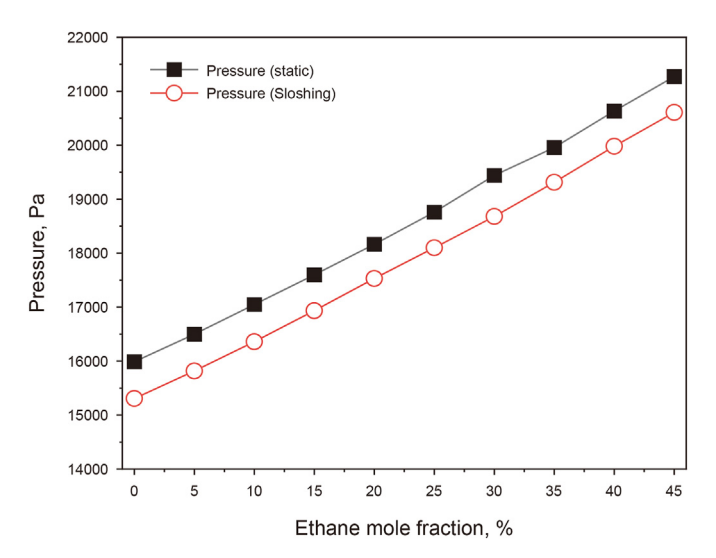


Fig. 17. Pressure with ethane mole fraction.

performance and pressure drop is shown in Fig. 19. It can be found from the figure that increasing the mole fraction of ethane can improve the comprehensive performance of the SWHE. The comprehensive performance under the sloshing condition is higher than that under the static state. This is because the heat transfer coefficient is improved and the pressure drop is reduced by the sloshing, the comprehensive performance is improved more.

## 3.2. The influence of vapor quality on heat transfer performance when the second component is a liquid phase

Since the boiling point of ethane is lower than that of propane, it is assumed that the second component is in the liquid phase, so propane is in the liquid phase. Propane remains in the liquid state during mass transfer because the temperature does not reach the boiling point of propane. Assuming that the second component propane is liquid and the mole fraction remains constant at 30%, the effects of the vapor quality *x* of the first component ethane on the heat transfer coefficient are studied.

As can be seen from Fig. 20, when the second component



Fig. 18. The interface of the liquid and gas.

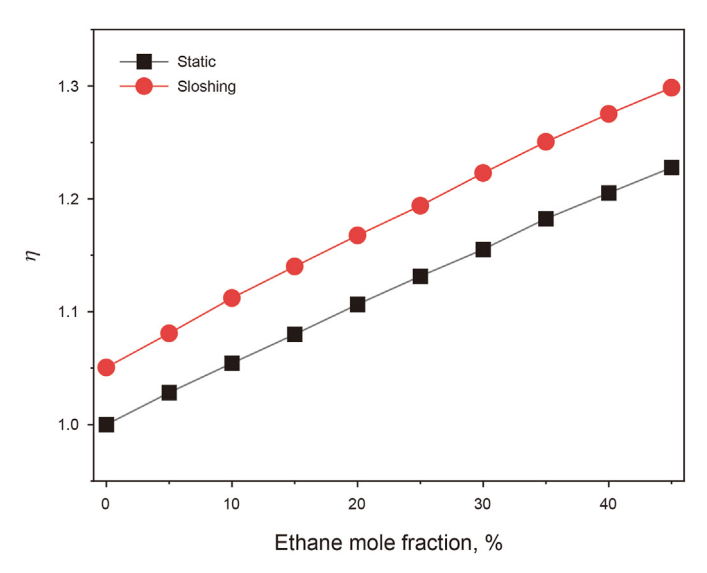


**Fig. 19.**  $\eta$  with different ethane mole fraction.

propane remains unchanged, with the increase of the vapor quality x of the first component ethane, the heat transfer coefficient decreases significantly from 1304.7 to 929.8 W(m $^2$ ·K) $^{-1}$ . After adding the sloshing conditions, when the vapor quality  $x \leq 0.25$ , the sloshing slightly deteriorates the heat transfer performance, and the heat transfer coefficient h decreases by no more than 0.5%. When the vapor quality  $x \geq 0.3$ , the sloshing condition can slightly increase the heat transfer performance, and the heat transfer coefficient h increases by no more than 0.7%. The simulation results here are similar to the conclusions of Ren et al. (2018a). For different working conditions, sometimes sloshing may not enhance the heat transfer performance and may deteriorate it.

This is because as the vapor quality increases, the proportion of the first component ethane in the liquid refrigerant decreases. The rate of energy transfer by sensible heat is far less than that by latent heat. Therefore, even under the same relaxation time, the temperature on the wall of the winding tubes will increase as the heat transfer rate decreases, resulting in the constant decrease of the heat transfer coefficient with the increase of vapor quality x. In addition, as the vapor quality x increases, the proportion of the gas phase increases and the velocity of the gas phase becomes faster, making it more difficult for liquid refrigerant to evenly cover the wall of winding tubes, as shown in Fig. 23.

As can be seen from Fig. 21, as the vapor quality x of the first component ethane increases, the relaxation time  $\beta$  also decreases from 2.02 to  $1.54~{\rm s}^{-1}$ . After adding the sloshing condition, when the vapor quality  $x \le 0.4$ , the sloshing can slightly increase the relaxation time  $\beta$ . In addition to the vapor quality of ethane of 0.05 and 0.3, the average relaxation time  $\beta$  increased by about 0.5%, and the improvement effect was very small. When the vapor quality  $x \ge 0.45$ , the sloshing condition begins to reduce the relaxation time  $\beta$  by about 0.25%.

This is due to the proportion of the first component ethane in the liquid refrigerant being lower and lower, and that of the gas phase being higher and higher. The velocity of the corresponding gas in the model between the winding tube layers is also faster and faster. As a result, the liquid phase between the winding tube layers is divided into two independent domains, and the thermal convection between the liquid phase ethane intensifies. However, the total amount of liquid ethane involved in mass transfer decreased, the mass transfer rate decreased gradually, and the relaxation time  $\beta$  also decreased. Fig. 24 is the section diagram of the control body at different positions along the cross-section of the winding tube. It can be seen from the figure that the cross sections are at different positions of the control body. The red gas phase refrigerant cuts apart the liquid phase refrigerant of the two adjacent layers of wound tubes, which also reduces the diffusion of refrigerant between the layers of wound tubes, leading to the decline of the heat transfer performance.

As can be seen from Fig. 22, the pressure drop decreases from 23592.6 to 13903.1 Pa as the vapor quality x of the first component (ethane) increases from 0.05 to 0.6. Adding the sloshing conditions can slightly reduce the pressure drop. Compared with the static condition, the pressure drop under sloshing conditions decreases by about 6.7%-8.6% with the increase of the vapor quality, which is quite significant.

The reasons for the reduction of pressure drop under sloshing

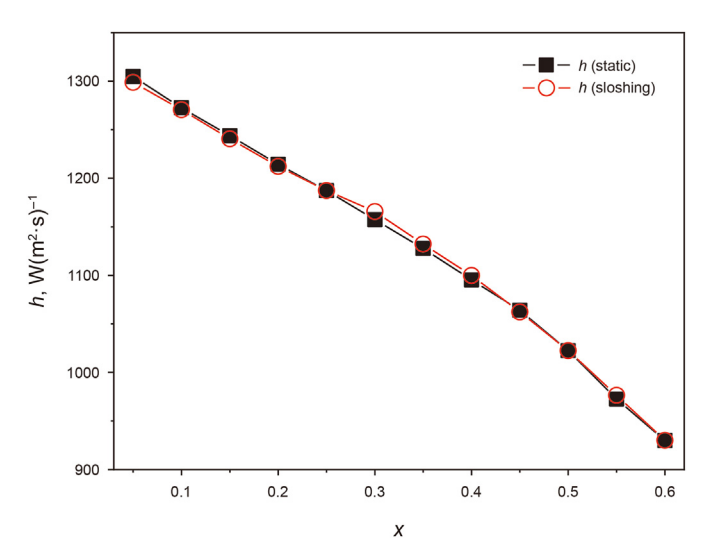


**Fig. 20.** Variations of h with x.

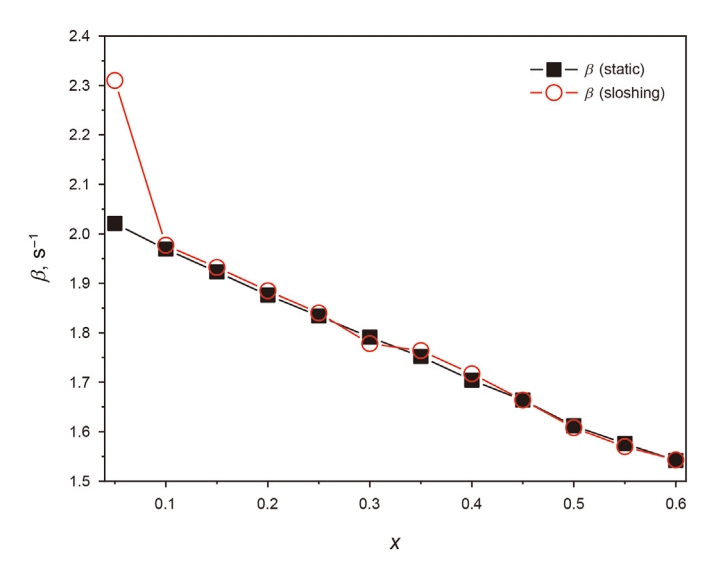


**Fig. 21.** Variations of  $\beta$  with x.

conditions are similar to those described above. Because the sloshing generates transverse, the lateral momentum generated by the sloshing facilitates the lateral migration of the refrigerant, thus reducing the pressure drop. As can be seen from Fig. 24((a)-(f)), the maximum longitudinal overflow area of the model shows a periodic change along the direction of the winding tubes. The sloshing conditions are conducive to the migration of the liquid refrigerant from a smaller flow area (Fig. 24(c)-(d)) to a larger flow area (Fig. 24(a) and (f)).

Although increasing the vapor quality reduces the heat transfer coefficient, it also reduces the pressure drop. To study the comprehensive influence of vapor quality on the heat transfer and pressure drop performance, a PEC (Performance evaluation criteria) is made on the heat transfer performance and pressure drop, as shown in Eq. (22).

$$\eta = \frac{Nu/Nu_0}{(f/f_0)^{1/3}} \tag{22}$$

The analysis results of PEC are shown in Fig. 25. It can be seen from the figure that the comprehensive performance of the SWHE

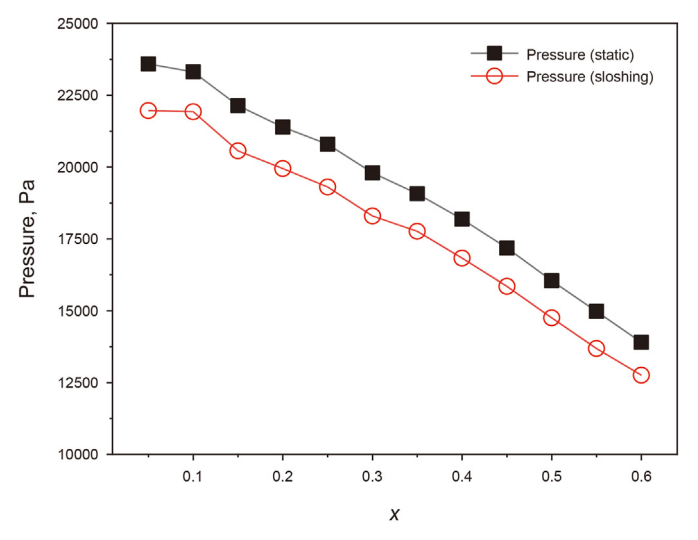


**Fig. 22.** Variation of pressure with *x*.

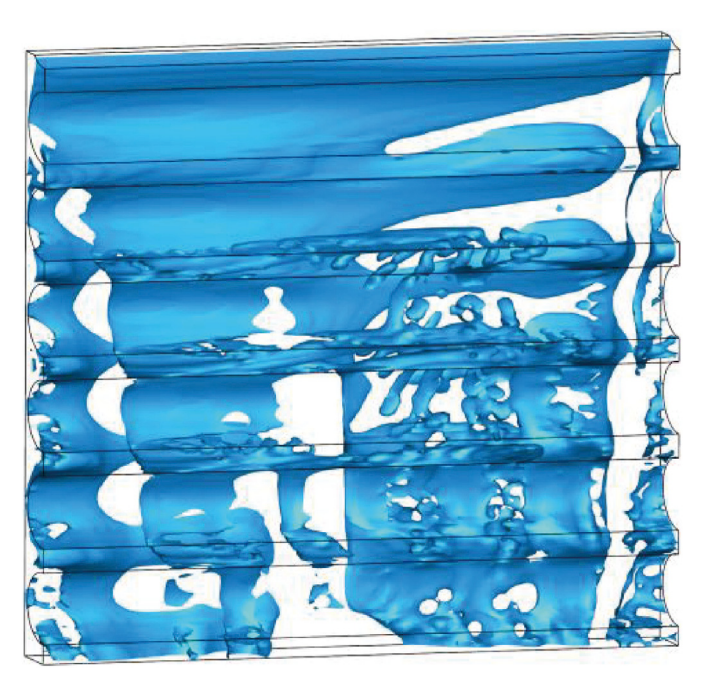


Fig. 23. The interface between liquid and vapor.

is improved with the increase of the vapor quality, but the comprehensive performance has been improved lower and lower, and when the vapor quality is about 0.5, the magnitude of the increase is very small. Compared with the static state, the sloshing condition can improve the overall performance, but the extent of the improvement is limited.

## 3.3. Influence of component proportion on heat transfer performance when the second component is a liquid phase

This part studies the influence of adjusting the mole ratio of the second component propane in the mixed refrigerant and adding the sloshing condition on the performance of SWHEs when the mass flow rate of the vapor and liquid phases remains unchanged. The mole ratio of the second component propane in the gas-liquid mixture refrigerant is 0–55%, and the mass fraction of propane in the liquid phase is 0–98.8%. The calculation results are shown in Figs. 26–28.

As can be seen from Fig. 26, with the increase of the mole fraction of the second component propane, the heat transfer coefficient h decreases gradually from 1180.2 to 1093.3 W ( $m^2 \cdot K$ ) $^{-1}$ . This is because the proportion of liquid ethane involved in mass transfer decreases with the increase of the mole ratio of the propane. Therefore, the proportion of latent heat to the total heat decreases, and the wall temperature of the winding tubes gradually increases with the decrease of the latent heat ratio, and then the heat transfer coefficient also decreases. Sloshing conditions can slightly enhance the heat transfer performance, increasing by about 0.1%-0.8%. This is mainly due to the fact that under sloshing conditions, the diffusion rate of liquid ethane in the mixture of ethane and propane is intensified, which indirectly accelerates the contact between ethane and the winding tubes and increases the mass transfer rate.

It can also be seen from Fig. 27 that the relaxation time  $\beta$ , which reflects the mass transfer rate, also decreases with the decrease of liquid ethane, from 1.89 to 1.68 s<sup>-1</sup>. This is consistent with the decrease of the heat transfer coefficient, mainly because with the increase of the mole ratio of the second component propane, the

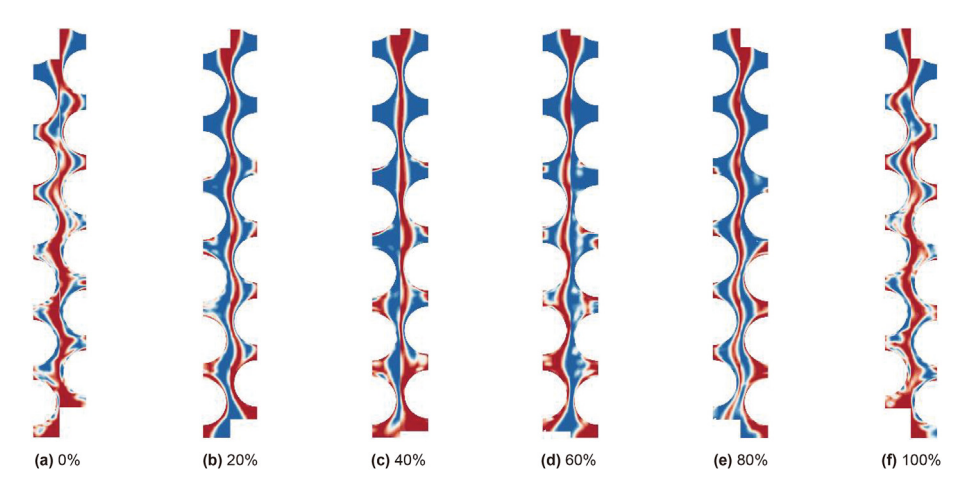
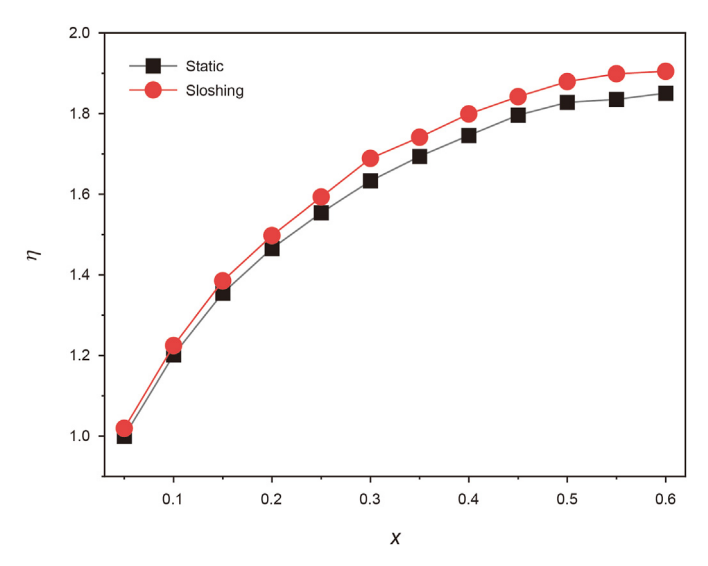
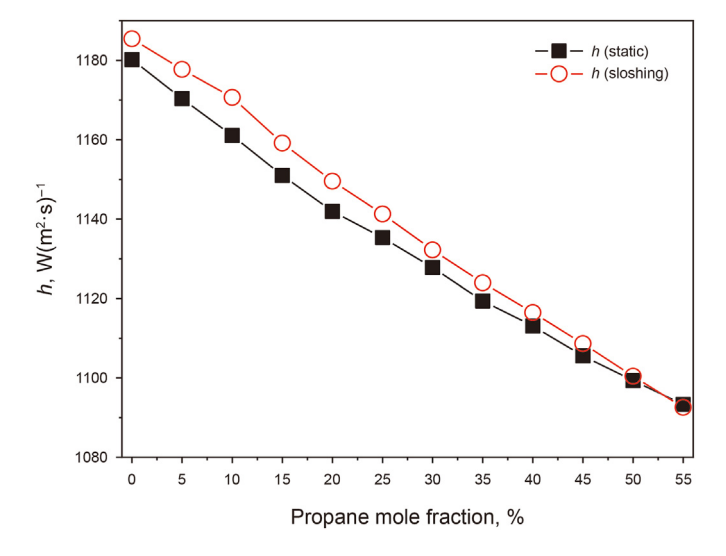


Fig. 24. Liquid and gas distribution of the cross-section at different locations.



**Fig. 25.**  $\eta$  with different x.



**Fig. 26.** h with propane fraction.

proportion of liquid ethane involved in mass transfer becomes lower and lower. Sloshing can slightly improve the relaxation time and mass transfer rate, and the relaxation time can be increased by about 0–0.8%. This is mainly because the diffusion rate of the liquid ethane in the mixed refrigerant composed of ethane and propane is accelerated under the sloshing condition, which indirectly accelerates the contact between ethane and the winding tubes and improves the mass transfer rate.

Combining Figs. 26 and 27, it can be found that with the increase of the molar ratio of propane, the increased heat transfer coefficient under sloshing conditions gradually decreases. The relaxation time is just the opposite, and it increases with the increase of the mole ratio of propane under sloshing conditions. This is because with the increase of the liquid propane and the decrease of the total amount of ethane, the effect of sloshing conditions on the diffusion of ethane in the mixed liquid phase decreases with the decrease of the proportion of ethane involved in mass transfer. So the increase of the heat transfer coefficient decreases. Compared with the static condition, as the proportion of liquid ethane decreases, the diffusion effect of the ethane in the mixed liquid phase becomes more and more obvious due to the sloshing conditions. Therefore, with the increase of the proportion of the second component propane which does not participate in mass transfer, the amplitude of the

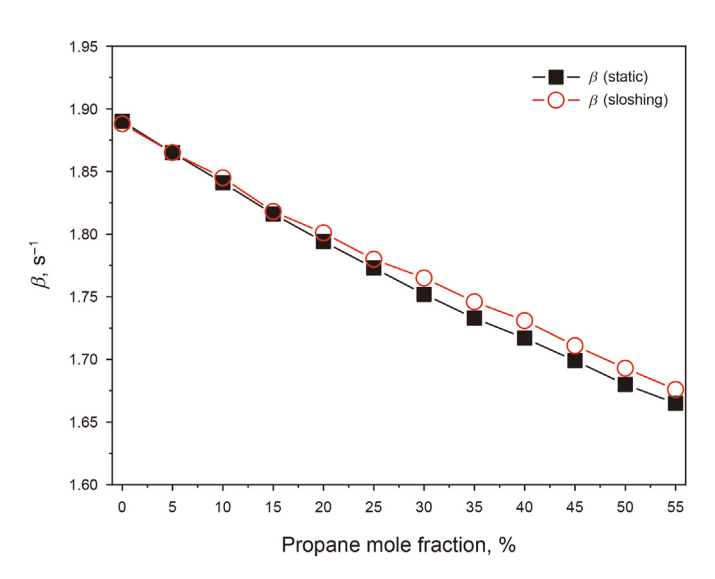


**Fig. 27.**  $\beta$  with propane fraction.

increase of the relaxation time by sloshing conditions is also gradually increasing.

As can be seen from Fig. 28, the pressure drop decreases from 22537.0 to 16766.3 Pa as the mole fraction of propane increases. Although the mass flow rates of the liquid and gas phases remain constant, the average density of the mixture composed of liquid ethane and propane continues to increase with the increase of the mole ratio of propane. Therefore, in the momentum equation, the proportion of the mass force gradually increases. The proportion of the viscous force gradually decreases, and the pressure drop gradually decreases. The sloshing reduces the pressure drop by about  $-5.4 \sim -7.9\%$ . As described above, this is still related to the lateral migration of liquid refrigerant under sloshing conditions.

Although increasing the mole fraction of propane reduces the heat transfer coefficient, it also reduces the pressure drop. To study the comprehensive influence of the mole fraction of propane on the heat transfer and pressure drop performance, the comprehensive performance (PEC) is computed, as shown in Fig. 29. As the propane mole fraction increases, the overall performance is improved, but the improvement is very limited. There is a slight improvement in the overall performance under sloshing conditions compared with the static condition.

#### 4. Conclusions

In the present study, the multi-component model in FLUENT and the self-defined sloshing condition are used to study the heat and mass transfer characteristics of gas-liquid two-phase mixed refrigerant on the shell side of the SWHE. The mathematical model under the sloshing condition is obtained through mathematical derivation. The shell-side heat and mass transfer characteristics of the SWHE with multi-component under sloshing conditions are studied. The following conclusions are obtained as follows.

- (1) With the increase of the mole ratio of ethane, the heat transfer coefficient increases gradually, which is nearly a linear increase. The relaxation time  $\beta$  increases gradually, and the mass transfer rate increases, but the increased range is relatively small. Pressure drop also increases gradually. The overall performance is improved with the increase of the mole ratio of the ethane.
- (2) When the propane is used as the second component of the liquid phase and the ethane gas-liquid two-phase flow as the

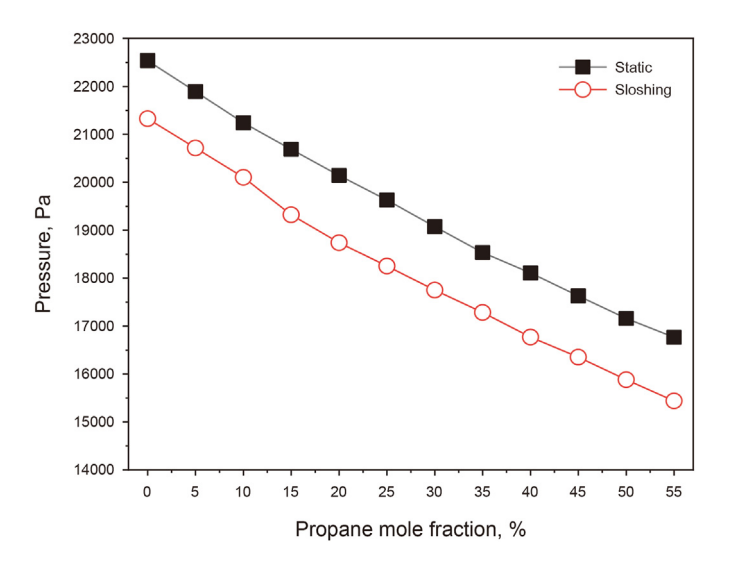
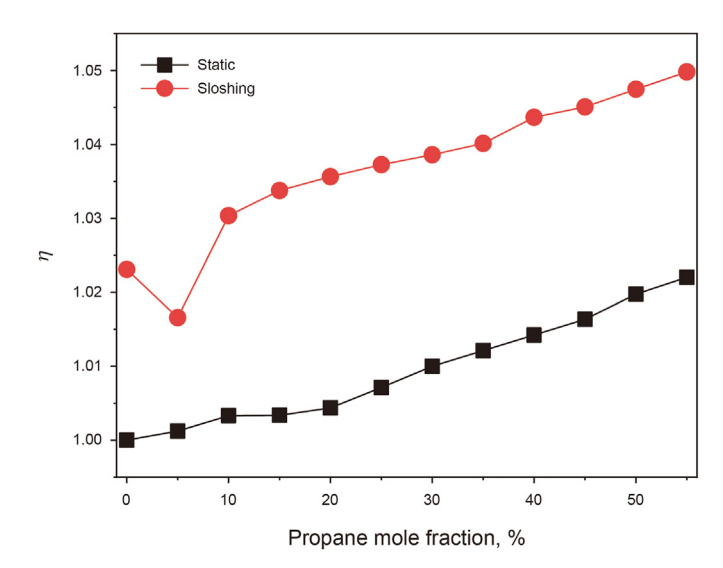


Fig. 28. Pressure with propane fraction.



**Fig. 29.**  $\eta$  with different propane fraction.

first component, the second component is kept constant. With the increase of vapor quality x, the heat transfer coefficient h, the relaxation time  $\beta$ , and the pressure drop decrease, respectively. The overall performance is improved with the increase in the vapor quality of the ethane.

- (3) With the propane as the second component of the liquid phase and the ethane gas-liquid two-phase flow as the first component, keeping the gas-phase ethane unchanged. The heat transfer coefficient h, the relaxation time  $\beta$ , and the pressure drop gradually decrease with the increase of the mole ratio of the propane refrigerant in the liquid phase, respectively. The overall performance is improved with the increase of the mole ratio of the propane.
- (4) The multi-component flow and heat transfer under sloshiing conditions is very complicated. The sloshing conditions sometimes can improve heat transfer performance and sometimes affect the heat transfer performance that is not obvious or even slightly degraded. When ethane is used as the second component of the gas phase and propane is used as the first component, the heat transfer coefficient and relaxation time  $\beta$  increase by 3.6%–4.6% under sloshing conditions. When propane is the second component of the liquid phase and ethane is the first, it is not obvious. When propane is used as the second component of the liquid phase and the ethane gas-liquid two-phase flow is used as the first component, The heat transfer performance improvement is about 0.1%–0.8%.
- (5) The reduction in pressure drop is consistent with the sloshing condition, which accelerates the lateral migration of liquid-phase refrigerant along the winding tube on the shell side of the SWHE and contributes to the reduction in flow resistance. The reduction of pressure drop under sloshing conditions is about −8.6% to −3.1%. Finally, considering both the heat transfer and pressure drop, the comprehensive performance of multi-component refrigerants has been improved, and the improvement is more significant under sloshing conditions.

#### **Declaration of competing interest**

The authors declare that they have no known competing financial interests or personal relationships that could have

appeared to influence the work reported in this paper.

#### Acknowledgments

This work was funded by the National Natural Science Foundation of China (No. 51806236, No. 51806239), the Fundamental Research Funds for the Central Universities (No. 2015XKMS059), Shaanxi Postdoctoral Fund Project (No. 2018BSHEDZZ56) and Foundation of Key Laboratory of Thermo-Fluid Science and Engineering (Xi'an Jiaotong University), Ministry of Education (No. KLTFSE2017KF01).

#### Nomenclature

$A_Z$	Amplitude of up and down undulating motion, mm
h	Convective heat transfer coefficient, $W \cdot m^{-2} \cdot K^{-1}$
$h_{\rm s\ ratio}$	Heat generation ratio
1	Swing arm, mm
m	Mass, kg
T	David of avving mation named disclar to the V avia

 $T_X$  Period of swing motion perpendicular to the *X*-axis, s  $T_Z$  Period of undulating motion in *Z*-axis, s

vol Temperature-weighted volume, m<sup>3</sup>·K

x Vapor quality, %

#### Greek symbols

 $\begin{array}{lll} \alpha & & \mbox{Volume fraction, \%} \\ \beta & & \mbox{Relaxation time, s}^{-1} \\ \varphi & & \mbox{Phase angle, }^{\circ} \end{array}$ 

 $\eta$  Comprehensive performance index

#### Subscripts

pre Previous

lv From a liquid phase to a vapor phase

liq Liquid phase vap Vapor phase

X Component in the x-direction
 Y Component in the y-direction
 Z Component in the z-direction

#### References

- Brackbill, J.U., Kothe, D.B., Zemach, C., 1992. A continuum method for modeling surface tension. J. Comput. Phys. 100, 335–354. https://10.1016/0021-9991(92)
- Ding, C., Hu, H.T., Ding, G.L., et al., 2017a. Experimental investigation on pressure drop characteristics of two-phase hydrocarbon mixtures flow in the shell side of LNG spiral wound heat exchangers. Appl. Therm. Eng. 127, 347–358. https:// 10.1016/j.applthermaleng.2017.08.025.
- Ding, C., Hu, H.T., Ding, G.L., et al., 2017b. Experimental investigation on downward flow boiling heat transfer characteristics of propane in shell side of LNG spiral wound heat exchanger. Int. J. Refrigeration-Revue Internationale Du Froid 84, 13–25. https://10.1016/j.ijrefrig.2017.08.006.
- Ding, C., Hu, H.T., Ding, G.L., et al., 2018. Influences of tube pitches on heat transfer and pressure drop characteristics of two-phase propane flow boiling in shell side of LNG spiral wound heat exchanger. Appl. Therm. Eng. 131, 270–283. https://10.1016/j.applthermaleng.2017.12.020.
- Duan, Z.D., Ren, T., Ding, G.L., et al., 2016. A dynamic model for FLNG spiral wound heat exchanger with multiple phase-change streams based on moving boundary method. J. Nat. Gas Sci. Eng. 34, 657–669. https://10.1016/j.jngse.

#### 2016.07.036.

- Duan, Z.D., Ren, T., Ding, G.L., et al., 2017. Liquid-migration based model for predicting the thermal performance of spiral wound heat exchanger for floating LNG. Appl. Energy 206, 972–982. https://10.1016/j.apenergy.2017.09.003.
- Han, H., Sun, C., Wang, Y., et al., 2017. Numerical simulation of horizontal tube falling film flow under tilt and sloshing conditions. Proc. 9th Int. Conf. Appl. Energy 3888–3894.
- Han, H., Wang, S.W., He, T., et al., 2019. Numerical study of the falling film thickness around the tube bundle with different spacings between spray holes and tubes under tilt and sloshing conditions. Int. J. Heat Mass Tran. 138, 184–193. https://10.1016/j.iiheatmasstransfer.2019.04.063.
- Hu, H.T., Ding, C., Ding, G.L., et al., 2019. Heat transfer characteristics of two-phase mixed hydrocarbon refrigerants flow boiling in shell side of LNG spiral wound heat exchanger. Int. J. Heat Mass Tran. 131, 611–622. https://10.1016/j.iiheatmasstransfer.2018.11.106.
- Lee, W.H., 1979. A Pressure Iteration Scheme for Two-phase Modeling. Technical Report.
- Li, J.R., Hu, H.T., Wang, H.X., 2020. Numerical investigation on flow pattern transformation and heat transfer characteristics of two-phase flow boiling in the shell side of LNG spiral wound heat exchanger. Int. J. Therm. Sci. 152. https://10.1016/j.ijthermalsci.2020.106289.
- Ren, Y., Cai, W.H., Chen, J., et al., 2018a. Numerical study on the shell-side flow and heat transfer of superheated vapor flow in spiral wound heat exchanger under rolling working conditions. Int. J. Heat Mass Tran. 121, 691–702. https://10.1016/i.iiheatmasstransfer.2018.01.025.
- Ren, Y., Cai, W.H., Chen, J., et al., 2018b. The heat transfer characteristic of shell-side film flow in spiral wound heat exchanger under rolling working conditions. Appl. Therm. Eng. 132, 233–244. https://10.1016/j.applthermaleng.2017.12.092.
- Ren, Y., Cai, W.H., Jiang, Y., 2018c. Numerical study on shell-side flow and heat transfer of spiral-wound heat exchanger under sloshing working conditions.
  Appl. Therm. Eng. 134, 287–297. https://10.1016/j.applthermaleng.2018.01.119.
  Ren, Y., Jiang, Y.Q., Cai, W.H., et al., 2018d. Numerical study on shell-side saturated
- Ren, Y., Jiang, Y.Q., Cai, W.H., et al., 2018d. Numerical study on shell-side saturated boiling heat transfer in spiral wound heat exchanger. Appl. Therm. Eng. 140, 657–670. https://10.1016/j.applthermaleng.2018.04.137.
- Ren, Y., Cai, W.H., Jiang, Y.Q., et al., 2022. Numerical study on the flow characteristic of shell-side film flow of floating LNG spiral wound heat exchanger. Int. J. Heat Mass Tran. 187. https://10.1016/j.ijheatmasstransfer.2021.122198.
- Sun, C.Z., Li, Y.X., Zhu, J.L., et al., 2017. Experimental tube-side pressure drop characteristics of FLNG spiral wound heat exchanger under sloshing conditions. Exp. Therm. Fluid Sci. 88, 194–201. https://10.1016/j.expthermflusci.2017.06.001.
- Sun, C., Li, Y., Han, H., et al., 2019a. Experimental study on shell-side pressure drop and offshore adaptability of LNG-FPSO spiral wound heat exchanger. Exp. Therm. Fluid Sci. 109, 1–16. https://10.1016/j.expthermflusci.2019.109874.
- Sun, C., Li, Y., Han, H., et al., 2019b. Experimental and numerical simulation study on the offshore adaptability of spiral wound heat exchanger in LNG-FPSO DMR natural gas liquefaction process. Energy 189, 1–12. https://10.1016/j.energy. 2019.116178
- Sun, C.Z., Li, Y.X., Han, H., et al., 2019c. Experimental study on shell-side pressure drop and offshore adaptability of LNG-FPSO spiral wound heat exchanger. Exp. Therm. Fluid Sci. 109. https://10.1016/j.expthermflusci.2019.109874.
- Sun, C.Z., Li, Y.X., Han, H., et al., 2019d. Experimental and numerical simulation study on the offshore adaptability of spiral wound heat exchanger in LNG-FPSO DMR natural gas liquefaction process. Energy 189. https://10.1016/j.energy. 2019.116178.
- Sun, C.Z., Cao, X.W., Li, Y.X., et al., 2021. Improvement of offshore adaptability of main cryogenic heat exchanger in FLNG dual mixed refrigerant liquefaction process. Int. J. Heat Mass Tran. 169. https://10.1016/j.ijheatmasstransfer.2021. 120909.
- Wang, T.T., Ding, G.L., Ren, T., et al., 2016. A mathematical model of floating LNG spiral-wound heat exchangers under rolling conditions. Appl. Therm. Eng. 99, 959–969. https://10.1016/j.applthermaleng.2016.01.138.
- Wu, Z., Liu, Y., Jian, W., et al., 2019. Numerical simulation of shell-side falling film boiling of LNG spiral wound heat exchanger. Chem. Ind. Eng. 36 (3), 72–79.
- Yan, Y., Sun, C.Z., Han, H., et al., 2019. Experimental study on thermal performance of FLNG spiral wound heat exchanger under sloshing conditions. J. Therm. Sci. 28 (5), 1042–1053. https://10.1007/s11630-019-1202-9.
- Yu, S.C., Chen, J., Mi, X.G., et al., 2019. Experimental and numerical investigation of two-phase flow outside tube bundle of liquefied natural gas spiral wound heat exchangers under offshore conditions. Appl. Therm. Eng. 152, 103—112. https:// 10.1016/j.applthermaleng.2019.02.051.